IEEE Photonics Journal
An IEEE Photonics Society Publication

Checkerboard Nanoplasmonic Gold Structure for Long-Wave Infrared Absorption Enhancement

Volume 6, Number 4, August 2014

Ehab Awad, Senior Member, IEEE
Mohamed Abdel-Rahman
Muhammad Fakhar Zia

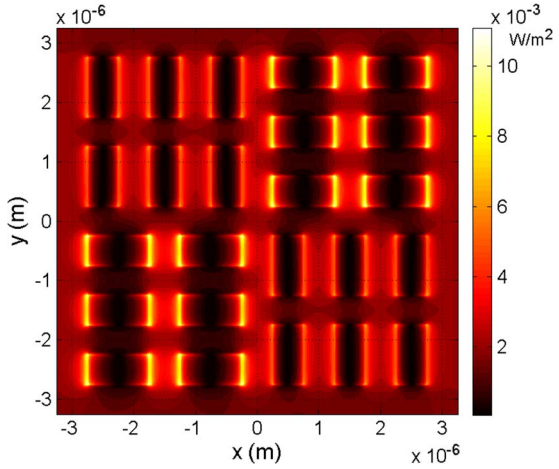

DOI: 10.1109/JPHOT.2014.2345879
1943-0655 © 2014 IEEE

Checkerboard Nanoplasmonic Gold Structure for Long-Wave Infrared Absorption Enhancement

Ehab Awad,[1] *Senior Member, IEEE*, Mohamed Abdel-Rahman,[2] and Muhammad Fakhar Zia[2]

[1]Department of Electrical Engineering, College of Engineering, King Saud University, Riyadh 11421, Saudi Arabia
[2]Prince Sultan Advanced Technologies Research Institute (PSATRI), College of Engineering, King Saud University, Riyadh 11421, Saudi Arabia

DOI: 10.1109/JPHOT.2014.2345879

Manuscript received June 4, 2014; revised July 30, 2014; accepted July 30, 2014. Date of publication August 6, 2014; date of current version August 13, 2014. This work was technically and financially supported by the Research Center of the College of Engineering and the Deanship of Scientific Research, King Saud University. Corresponding author: E. Awad (e-mail: esawad@ieee.org).

Abstract: A localized nanoplasmonic induced absorption enhancement in silicon nitride (Si_3N_4) dielectric material using a nanoscale novel checkerboard gold (Au) structure is demonstrated. The checkerboard structure is fabricated on a Si_3N_4 layer using electron-beam lithography and sputter deposition techniques. The plasmonic electric field and optical absorption enhancement are measured using scanning near-field optical microscopy. Finite-difference time-domain simulations are utilized to characterize the absorption spectral response enhancement together with its dependence on incidence angle and polarization. The checkerboard shows a broadband average spectral absorption enhancement of 63.2% over the wavelength range 8–12 μm with a maximum enhancement of 107% at 8 μm and a minimum enhancement of 24.8% at 12 μm. The degradation of enhanced absorption with incidence angle variation (0°–60°) is less than 1.6% at 10.6-μm wavelength. The checkerboard device shows polarization-independent absorption enhancement with incidence angles.

Index Terms: Nanophotonics, plasmonics, long-wave infrared absorption.

1. Introduction

Surface plasmons take place when light electromagnetic waves interact with a sub-wavelength metal object resulting in conduction electrons oscillations. The oscillating electrons give rise to nano-plasmonic electric field that becomes confined within sub-wavelength resolution areas near the metal with very high magnitude. This phenomenon has recently found many applications in plasmonic waveguides, enhanced transmission through apertures, enhanced photoluminescence and Raman scattering for spectroscopy [1], [2].

Recently, some groups have reported on surface plasmon enhanced absorption in the long-wave infrared (LWIR) range with potential applications in photodetectors and microbolometers. For example, surface plasmon waves were used to enhance detectivity of quantum-well infrared detectors by using periodic array of holes in an Au thin film [3]. Also, surface plasmon waves were used to enhance detectivity of quantum-dot infrared detectors for focal plane arrays using corrugated Au metal and metal photonic crystal [4]. Long wave infrared focal plane array with

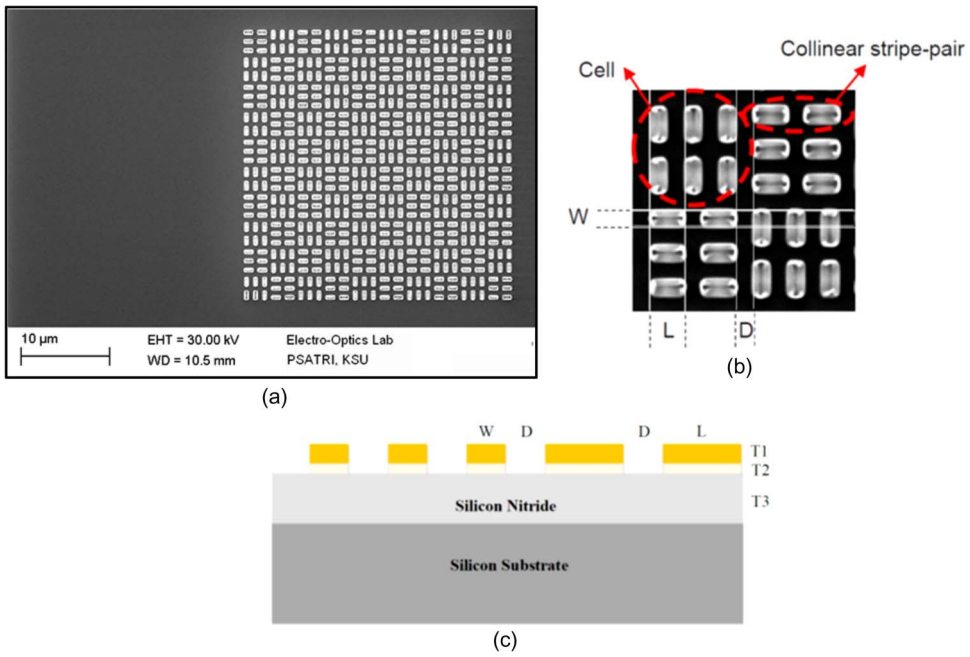

Fig. 1. (a) The SEM image (Top-view) of the fabricated checkerboard device sample $(30 \times 30\ \mu m^2)$. (b) Magnified SEM image of fabricated four cross-oriented cells, L = 1049 nm, D = 530 nm, W = 510 nm. (c) A schematic cross-section in the device layer structure with two cross-oriented cells, L = 1000 nm, W = 500 nm, D = 500 nm, T1 (Au) = 50 nm, T2 (Ti) = 10 nm, T3 (Si_3N_4) = 400 nm.

enhanced noise-equivalent temperature difference was demonstrated by using backside configured sub-wavelength hole-array plasmonic structure [5]. Moreover, concentric double C-shaped plasmonic structure was used to enhance the optical absorption in uncooled microbolometer pixels [6], [7].

In this work, we demonstrate a novel nanoscale checkerboard Au structure that can enhance optical absorption of LWIR radiation in underneath dielectric material by induced localized surface plasmons. The checkerboard structure consists of Au stripes that act as sub-wavelength optical antennas where oscillating electrons accumulate at the stripe edges resulting in a spatial nano resolution enhanced electric field [8]. The localized surface plasmons accumulate optical energy and enhance quality-factor in the vicinity of metal resulting in concentrated high optical intensities [2]. The potential applications of checkerboard structure are LWIR photodetectors and microbolometers, where absorption enhancement is mandatory to increase device responsivity.

2. The Checkerboard Structure

The checkerboard structure is a 2D array of cells with Au nanoscale stripes ($1000 \times 500 \times 50$ nm), as shown in Fig. 1. Each cell consists of parallel pairs of collinear-stripes that are separated by sub-wavelength gaps. The parallel stripe-pairs are also separated by sub-wavelength gaps. The cells are arranged within the array in periodically alternating orthogonal-orientations (i.e., cross-oriented cells) to ensure polarization-independent spectral-response of the structure.

The checkerboard plasmonic structure was fabricated on silicon (Si) substrate having a 400 nm thick layer of silicon-nitride (Si_3N_4) deposited by plasma enhanced chemical vapor deposition (PECVD) technique. The Si_3N_4 layer acts as an absorbing dielectric layer underneath the checkerboard structure. It has a refractive index of "1.97 + 1.37i" at 10.6 μm wavelength. Patterning of the checkerboard structure was done by electron-beam lithography using a modified ZEISS MA10 scanning electron microscope (SEM) with Raith Elphy Quantum nanolithography module. The SEM's LaB6 cathode was operated at an accelerating voltage of 30 kV. The exposure current

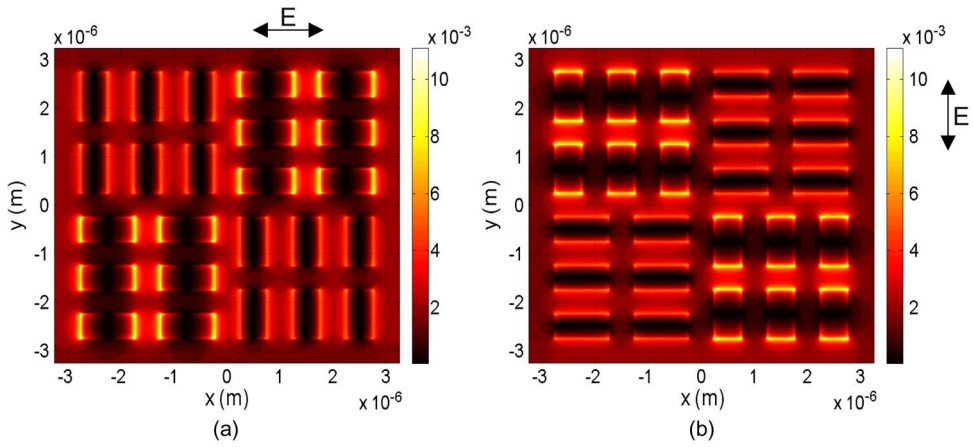

Fig. 2. The FDTD simulations of field intensities (W/m^2) of four cross-oriented cells at 10.6 μm wavelength with normal incident plane-wave for (a) TM and (b) TE polarization. The arrows indicate the electric field polarization.

was 11.5 pA. A bilayer resist process was used. The bottom layer is a 350 nm of copolymer methyl methacrylate–methacrylic acid (MMA–MAA) baked for 10 min on a hotplate at 180 °C. The top layer is 150 nm of 495-K polymethyl methacrylate (PMMA) baked for 10 min on a hotplate at 180 °C. The checkerboard structures were exposed in a 100×100 μm^2 write field at an area dose of 315 $\mu C/cm^2$ and 1 μs of dwell time. The resist was then developed for 30 s in a 1 : 3 mixture of methylisobutylketone:isopropanol (MIBK:IPA). After patterning the checkerboard, a 10 nm thick film of Titanium (Ti) was deposited using DC sputtering at 150 W of power at a chamber base pressure of 2×10^{-6} Torr and Argon pressure of 3 mTorr. Immediately afterwards, 50 nm of Au were deposited using DC sputtering at the same sputtering conditions that were used for depositing Ti. Liftoff was then performed to remove all the excess metal and ending with the plasmonic checkerboard structures.

Fig. 1(a) shows a scanning electron microscope (SEM) image of checkerboard device sample with a total area 30×30 μm^2. Fig. 1(b) shows a magnified SEM image of four cross-oriented cells on the sample along with dimensions and marked pair of collinear-stripes. Fig. 1(c) shows a schematic cross-section of the designed device with two cross-oriented cells along with thin-film layers materials and their thickness. It worth mentioning that the designed sub-wavelength stripes dimensions are equivalent to $L = \lambda/10$, $W = D = \lambda/20$, $T1 = \lambda/200$ at the wavelength of $\lambda = 10$ μm.

3. FDTD Simulations

In order to theoretically analyze and characterize the checkerboard structure, a three dimensional finite-difference time domain (FDTD) simulations are performed using Lumerical software [9]. The optical parameters of the device materials are obtained from the software library, while the (Si_3N_4) refractive-index together with its dependence on wavelength are obtained from [10]. Fig. 2 shows the plasmonic intensity distribution on (Si_3N_4) layer surface due to four cross-oriented cells of checkerboard structure in the case of TM (Fig. 2(a)) and TE (Fig. 2(b)) polarized normal-incident plane-waves at wavelength of 10.6 μm. The incident electric field on the sub-wavelength Au stripes induces collective conduction electron oscillations (dipoles) in the direction of polarized incident electric-field [1], [2]. The oscillating charges accumulate at stripes edges and corners creating a localized surface plasmon high field and intensity in the vicinity of metal. The confined electric field has the highest intensity at stripe corners, followed by less intensity at stripe edges that are perpendicular to incident electric field polarization. In addition, the stripe aspect-ratio (2 : 1) allows the narrow-edges to develop much higher intensities than stripe wide-edges. The sub-wavelength gaps between Au stripes result in coupled plasmonic fields (in-phase oscillating dipoles), and thus more enhanced optical intensities within the gaps

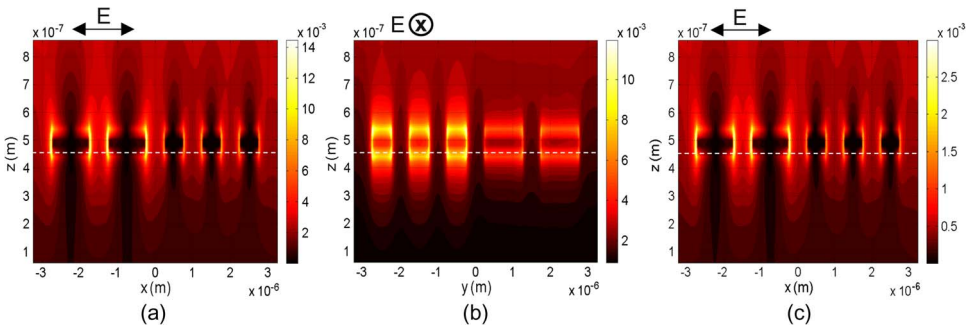

Fig. 3. Vertical distributions of field intensities (W/m^2) of two cross-oriented cells at 10.6 μm wavelength with normal incidence and TM polarization at cross-section planes: (a) Y $= -250$ nm, and (b) X $= -250$ nm of Fig. 2. (c) 60° incidence angle, Y $= -250$ nm. The dotted white lines indicate the upper-surface of silicon-nitride layer. The arrows indicate electric field polarization.

(hot-spots). The maximum intensity shown in Fig. 2(a), is almost 12-times more than that of same device without checkerboard. It is worth mentioning that the intensity distribution in Fig. 2 (b) for TE case looks similar to that in Fig. 2(a) for TM case with 90° rotation, because of the cross-oriented cells configuration. This indicates that the same amount of optical power is collected by the total device area for each polarization, and thus the device is polarization-independent. It is worth mentioning that the field intensity is directly related to the optical power absorption, besides it has the same distribution as the electric field magnitude which is simply proportional to the square root of intensity.

Fig. 3 shows vertical cross-section in plasmonic intensity distribution of two cross-oriented cells for the case of TM normal-incident plane-wave at 10.6 μm wavelength. The two cross-section planes are chosen at the positions Y $= -250$ nm and X $= -250$ nm in Fig. 2(a), to include the stripes edges. Whereas the TM is chosen as a polarization example for a polarization-independent device. The two selected cross-sections cover the entire (Si_3N_4) layer as well as part of the air above the device. The horizontal dotted white lines in Fig. 3 indicate the upper surface of the (Si_3N_4) layer. As seen, the intensity spreads inside the (Si_3N_4) and almost vanishes at the layer bottom-surface, indicating absorption of most transmitted optical power inside this layer. The hot-spots are clear in Fig. 3(a), with highest intensities in the gaps between coupled collinear-stripes (on left-hand side). Fig. 3(c) shows one example of vertical field intensity distribution at incidence angle of 60° at the cross-section plane Y $= -250$ nm when the sample is illuminated by a far plane-wave source with TM polarization and 10.6 μm wavelength. It indicates reduction of intensity distribution (W/m^2) by approximately 0.2 factor when compared to the normal incidence case in Fig. 3(a).

Fig. 4(a) shows the absorption spectral-response of the device within the 8–12 μm wavelength range for both cases of TE and TM polarizations at normal incidence with/without checkerboard. The absorption here is defined as the ratio of total absorbed power to total incident power. It is obvious that the spectral response has increased over the entire wavelength range while maintaining the response shape, indicating a broadband enhancement. Although the plasmonic filed distribution should be dependent on TM and TE polarizations as already shown in Fig. 2, the absorption improvement is polarization-independent because of the cross-oriented checkerboard cells. The calculated average absorption over this wavelength range in the case of checkerboard is 18%, and in the case without checkerboard is 12.25%, corresponding to 5.75% improvement in average absorption. Fig. 4(b) shows the amount of absorption improvement (difference) for different wavelengths inside this range. The maximum absorption-difference is 7.5% at 10.2 μm wavelength. The absorption enhancement is defined here as the ratio between absorption-difference to absorption without checkerboard. The checkerboard shows an average spectral absorption enhancement of 63.2% over the entire wavelength range with a maximum of 107% at 8 μm and a minimum of 24.8% at 12 μm.

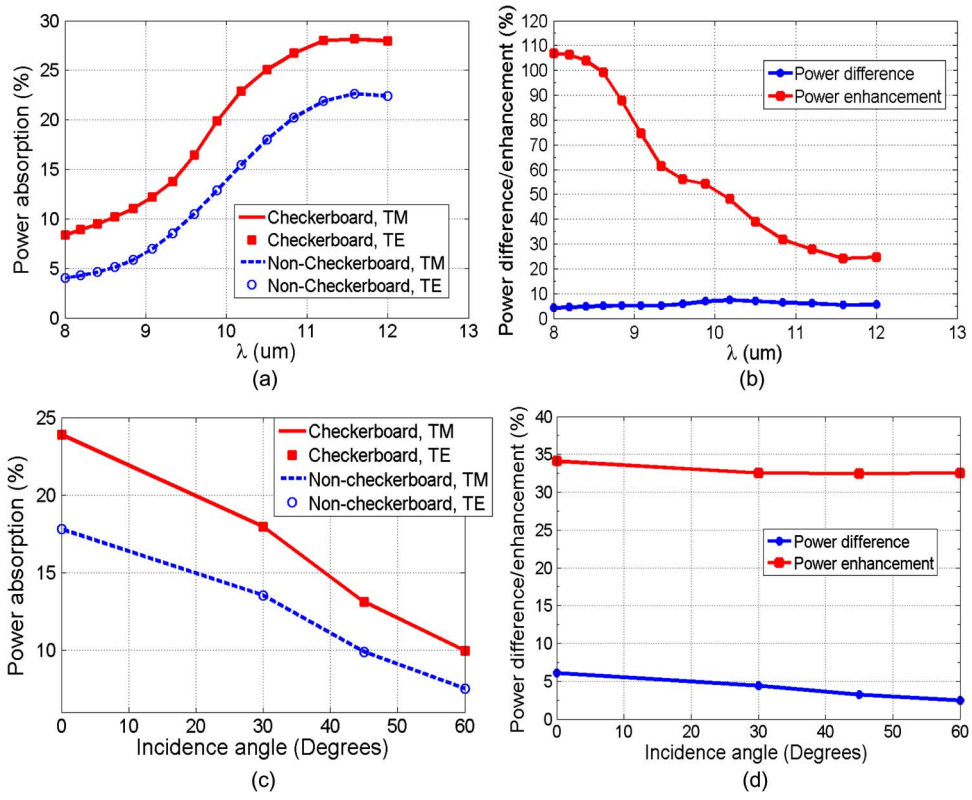

Fig. 4. (a) The absorption spectral-response of the device at normal incidence. (b) The difference and enhancement in absorption spectral-response. (c) The change in absorption with incidence angle at 10.6 μm wavelength, (d) The difference and enhancement in absorption with incidence angle at 10.6 μm wavelength.

Fig. 4(c) shows the change in absorption with incidence angle (0° to 60°) at 10.6 μm wavelength for both cases of TE and TM polarizations with/ without checkerboard. The change in enhanced absorption with incident angle is polarization-independent. Fig. 4(d), shows both the difference and enhancement in absorbed power as a function of incidence-angle. When the incidence-angle changes from 0° to 60°, the enhanced total absorption degrades by only 1.56%, on the other hand, the total absorption without checkerboard degrades by as much as 3.6%. It is worth mentioning that the calculated absorption in the Au checkerboard layer alone is less than 1.5% for all LWIR range and incidence angles. Which can be considered negligible when compared to the calculated total absorption in Fig. 4(a) and (c). That indicates most of incident power absorption occurs in the Si_3N_4 layer.

4. Testing and Measurements

Testing and measurements of induced plasmonic electric field for checkerboard device sample is performed using commercial scattering-type scanning near-field optical microscope (SNOM) [11]. The microscope operates in the reflection mode. For sample excitation, a LWIR illumination unit (CO_2 laser) was used to irradiate the sample at 60° incidence-angle. To collect the scattered near-field, a pseudo-heterodyne detection module was used [12]. A conventional silicon cantilever tip coated with platinum-iridium (Pt-Ir) acted as scattering near-field probe with a lateral resolution of 10 nm. To suppress any background contributions, the detected optical signal was demodulated at higher harmonics of the cantilever oscillation frequency [12].

Fig. 5(a) shows the electric field magnitude in arbitrary units (a.u.), which is scattered off the checkerboard sample. The incident field is TM polarized as indicated on the figure with 10.19 μm

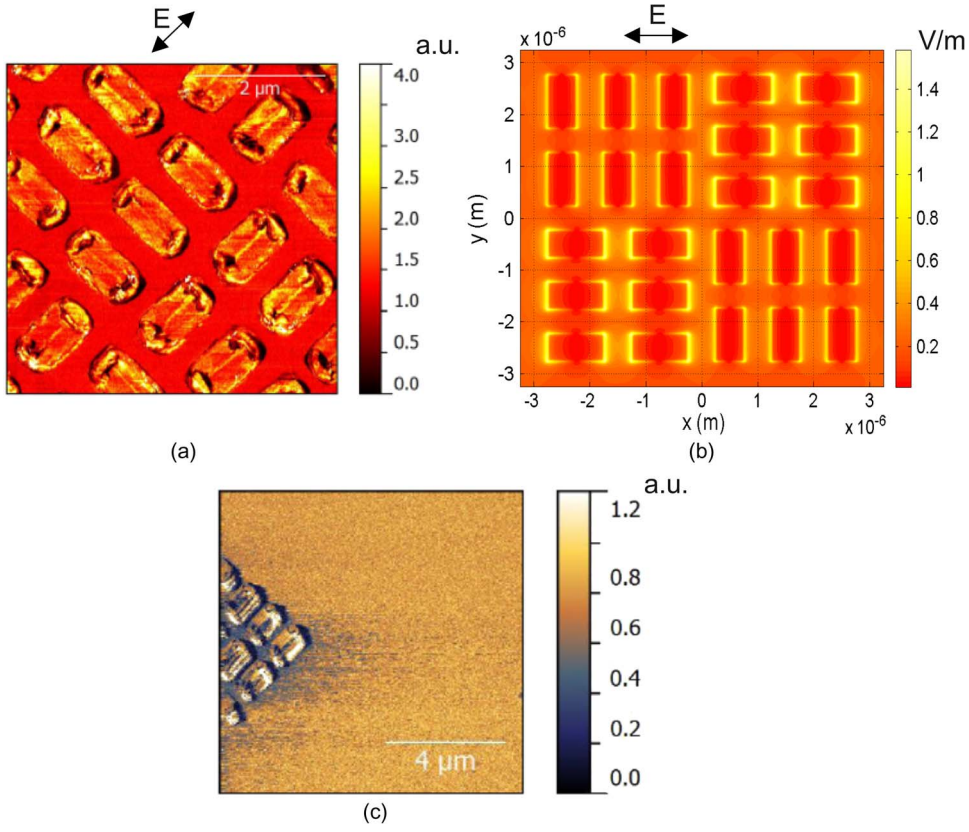

Fig. 5. (a) The SNOM image of the electric field magnitude scattered off the checkerboard sample (rotated) at 10.19 μm wavelength with TM polarization. (b) The FDTD simulation of scattered electric field magnitude under same SNOM measurement conditions in part 'a'. (c) A comparison of the SNOM scattered electric field magnitudes with/without checkerboard on the same sample at 10.6 μm wavelength.

wavelength and 60° incidence-angle. On average, the highest field magnitude at the Au stripes (3.3 a.u.) is almost 2.54-times that at silicon-nitride surface (1.3 a.u.). Fig. 5(b) shows the simulated checkerboard device under the same measurements conditions. On average, the highest field magnitude at Au stripes (1.2 V/m) is almost 2.4-times that at the (Si_3N_4) surface (0.5 V/m), which is in a good agreement with SNOM measurement. It is worth mentioning that the irregular field-magnitude distribution over Au stripes in SNOM measurement (Fig. 5(a)) is due to fabrication imperfections such as stripes round-corners, un-sharp edges, and residual e-beam resist, caused by limitations of available equipment and materials in our lab. Fig. 5(c) shows a measurement comparison between SNOM scattered field, at 10.6 μm wavelength, from the checkerboard area and that from a neighbor area on the same sample without checkerboard. On average, the scattered field magnitude at the golden-colored area without checkerboard (0.8 a.u.) is almost 1.6-times that at the dark area underneath the checkerboard (0.5 a.u.). This difference is due to enhanced power absorption in the checkerboard area (i.e., less scattered electric field). The variation in field magnitudes corresponds to a change in absorbed optical power equals $(1.6)^2 = 2.56$, which agrees very well with the simulation results in Fig. 4(d) (lower-curve) at 60° incidence-angle.

5. Conclusion

A novel gold checkerboard plasmonic structure for optical absorption enhancement in the LWIR is tested and characterized both numerically and experimentally. It shows an average spectral

enhancement of 63.2% with polarization-independent operation and very small degradation with incidence-angle variations. Silicon-nitride has been chosen here as an example of an absorbing dielectric layer underneath checkerboard structure. However with other dielectric materials that have comparable refractive-indices, it is expected to have a similar enhanced absorption. Besides, it is expected to have a comparable or maybe better performance with higher refractive-index materials (e.g. Si, Gallium-Arsenide (GaAs), Germanium (Ge), etc.) which can give more red-shift of plasmonic resonance [1] into LWIR region, and thus higher plasmonic fields. The ease of fabrication of the plasmonic checkerboard structure besides its excellent characteristics in the LWIR range promotes its use for absorption enhancement in photodetectors and microbolometers.

Acknowledgement

The authors would like to gratefully acknowledge Dr. Miriam Böhmler for her collaboration, efforts, and generous help in taking samples measurements using NeaSpec SNOM microscopy system.

References

[1] S. A. Maier, *Plasmonics: Fundamentals and Applications*. New York, NY, USA: Springer-Verlag, 2007.
[2] S. V. Gaponenko, *Introduction to Nanophotonics*. Cambridge, U.K.: Cambridge Univ. Press, 2010.
[3] W. Wu, A. Bonakdar, and H. Mohseni, "Plasmonic enhanced quantum well infrared photodetector with high detectivity," *Appl. Phys. Lett.*, vol. 96, no. 16, pp. 161107-1–161107-4, Apr. 2010.
[4] S. C. Lee, S. Krishna, and S. R. J. Brueck, "Plasmonic-enhanced photodetectors for focal plane arrays," *IEEE Photon. Technol. Lett.*, vol. 23, no. 14, pp. 935–937, Jul. 2011.
[5] J. Vaillancourt, N. Mojaverian, and X. Lu, "A longwave infrared focal plane array enhanced by backside-configured plasmonic structures," *IEEE Photon. Technol. Lett.*, vol. 26, no. 8, pp. 745–748, Apr. 2014.
[6] S. Z. Lulec *et al.*, "An analysis for the broadband absorption enhancement using plasmonic structures on uncooled infrared detector pixels," in *Proc. SPIE*, 2012, vol. 8353, pp. 83531D-1–83531D-8.
[7] O. Erturk, E. Battal, S. E. Kucuk, A. K. Okyay, and T. Akin, "A plasmonically enhanced pixel structure for uncooled microbolometer detectors," in *Proc. SPIE, Infrared Technol. Appl. XXXIX*, Jun. 2013, vol. 8704, pp. 87041E.
[8] Q. Park, "Optical antennas and plasmonics," *Contemp. Phys.*, vol. 50, no. 2, pp. 407–423, 2009.
[9] *Lumerical FDTD solutions*, [Online]. Available: www.lumerical.com
[10] J. Kischkat *et al.*, "Mid-infrared optical properties of thin films of aluminum oxide, titanium dioxide, silicon dioxide, aluminum nitride, and silicon nitride," *Appl. Opt.* 51, no. 28, pp. 6789–6798, Oct. 2012.
[11] *NeaSNOM*, [Online]. Available: www.neaspec.com
[12] N. Ocelic, A. Huber, and R. Hillenbrand, "Pseudoheterodyne detection for background-free near-field spectroscopy," *Appl. Phys. Lett.*, 89, no. 10, pp. 101124-1–101124-3, Sep. 2006.